SCIENCE CHINA
Information Sciences

• RESEARCH PAPERS •

October 2010 Vol. 53 No. 10: 1963–1976
doi: 10.1007/s11432-010-4075-9

Color image enhancement based on HVS and PCNN

ZHANG YuDong, WU LeNan*, WANG ShuiHua & WEI Geng

School of Information Science & Engineering, Southeast University, Nanjing 210096*, China*

Received November 5, 2008; accepted September 2, 2009

Abstract To enhance color images more effectively, a novel strategy is presented in this paper. We firstly translate the image to be enhanced from RGB space into HIS space, secondly keep its H component unchanged, and thirdly stretch its S component exponentially, and at last process its I component in the following manner: couple both the gray value and the spatial information into an inner activity item of corresponding neuron, integrate the human visual system into a dynamic component of corresponding neuron, and compare the inner activity item with dynamic component to obtain the enhanced image. Experiments demonstrate the effectiveness and validity of our strategy.

Keywords image enhancement, human visual system (HVS), pulse coupled neural network (PCNN), color image

Citation Zhang Y D, Wu L N, Wang S H, et al. Color image enhancement based on HVS and PCNN. Sci China Inf Sci, 2010, 53: 1963–1976, doi: 10.1007/s11432-010-4075-9

1 Introduction

Image enhancement is a basic low-layer processing means of making the blurred image clear and emphasizing interesting features. However, its original function is to enhance recognition ability of human eyes or computers rather than enhance the original information.

Classical enhancement methods, such as local statistics, histogram equalization (HE), and adaptive image contrast enhancement [1–3], cannot be totally automatic as they need the human invention more or less, nor can they enhance the global and local contrast at one time.

To solve these problems, a novel enhancement method based on pulse coupled neural network (PCNN) [4] and human vision system (HVS) is proposed.

The remainder of this paper is as follows: Section 2 introduces the rudimental concept of PCNN. Section 3 addresses the visual threshold effect, spatial concealment effect, and Mach effect. Section 4 modifies the classical visual threshold effect—Weber's law. Section 5 presents a global enhancement method based on modified visual threshold effect. Section 6 presents a local enhancement method based on spatial concealment effect and Mach effect, discusses the global and local enhance method, and extends it to color image enhancement. Sections 7 and 8 are digital experiments with gray-level images and color images respectively. Section 9 analyzes the consumed time. Finally section 10 concludes the paper.

*Corresponding author (email: wuln@seu.edu.cn)

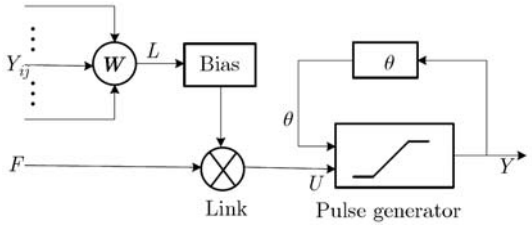

Figure 1 Neuromime of PCNN.

2 Model of PCNN

The studies on the pulse train synchronization vibration of a cat's visual cortical neuron by Eckhorn and his colleagues [4] in the last decade gave rise to the mammal's neuron model, and the PCNN model. This model can classify pixels of similar gray values, reduce the differences in local gray values, and remedy local minor gaps. So it has been widely applied to image processing field.

Figure 1 is an outline of neuromime, which consists of input, nonlinear link, and pulse-produce. It can be expressed by the following discrete equations [5, 6]:

$$F_{ij}[n] = \exp(-\alpha_F)F_{ij}[n-1] + V_F \sum m_{ijkl}Y_{kl}[n-1] + I_{ij}, \tag{1}$$

$$L_{ij}[n] = \exp(-\alpha_L)L_{ij}[n-1] + V_L \sum \omega_{ijkl}Y_{kl}[n-1], \tag{2}$$

$$U_{ij}[n] = F_{ij}[n](1 + \beta L_{ij}[n]), \tag{3}$$

$$Y_{ij}[n] = \begin{cases} 1, & U_{ij}[n] > \theta_{ij}[n-1], \\ 0, & U[n] \leqslant \theta_{ij}[n-1], \end{cases} \tag{4}$$

$$\theta_{ij}[n] = \exp(-\alpha_\theta)\theta_{ij}[n-1] + V_\theta Y_{ij}[n-1]. \tag{5}$$

Here, i and j are indices of neurons; n is iterative steps; I is external input; F is feedback input; L is linking input; U is inner activity; θ is a dynamic threshold; M and W are linking weight matrices (usually $M = W$); V_F, V_L and V_θ correspond to the magnitude constants of F, L, θ; α_F, α_L and α_θ are corresponding decay constants; β is the linking coefficient. Y is the binary output of PCNN.

The whole working process is as follows: if there is a pulse output, then the threshold will increase such that there will be no output during the next step. Therefore the threshold will exponentially decrease until it becomes smaller than the inner activity U, when there is another pulse output. The above processes cycle all the time.

3 Human vision system

3.1 Visual threshold effect (VTE)

As can bee seen in Figure 2, the fixed background light of intensity I_B is contained at a visual angle of 1.5° while the outside area is called environment with the intensity I_s. The area cycled by the dashed line is called stimuli area with intensity $I_B + \Delta I$.

ΔI is the difference in intensity just noticeable for an individual, called the "*difference threshold*".

Experiments show that ΔI is related to I_B. The most famous law for depicting the phenomenon is Weber's Law, which indicates that ΔI increases linearly with I_B if $I_B = I_s$.

However, the human perceptual optical spectrum can be divided into three parts: scotopic vision, mesopic vision, and photopic vision. Weber's law is only suitable for the photopic vision but not suitable for mesopic vision and scotopic vision. Thus, it is modified in section 4.

3.2 Spatial concealment effect (SCE)

When the brightness of the background in Figure 2 are not fixed, i.e. vary largely, the difference threshold will arise, which is called the spatial concealment effect.

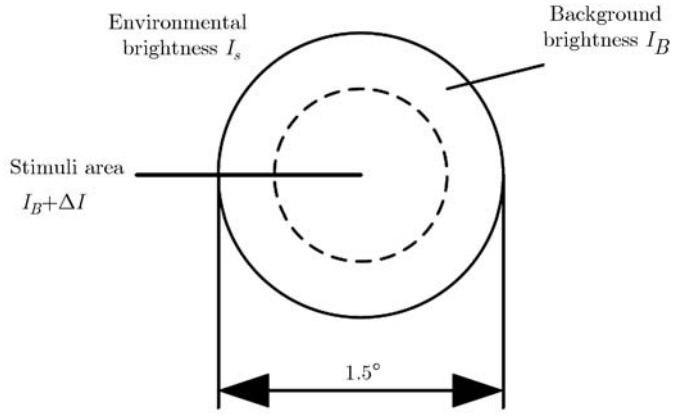

Figure 2 Experiments validating Weber's law.

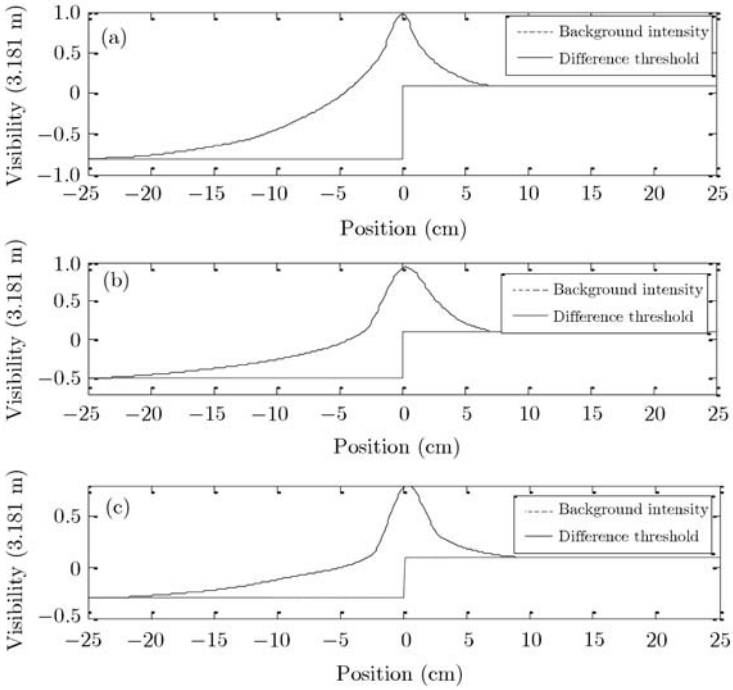

Figure 3 The curve of difference threshold with the position of the strip. (a) I_R/I_L=27.5; (b) I_R/I_L =8.7; (c) I_R/I_L =2.75.

A typical experiment is carried out where the brightness of the background is stepped-incremental along the horizontal direction. Suppose that the intensity of the left dark area and the right bright area are I_L and I_R respectively. The stimuli stripe is moved from left to right when the difference threshold is recorded. We can find that the difference threshold increases when the strip is near to the edge of the background, and their relationship is shown in Figure 3. If the x-axis is changed into the distance between the strip and the edge, the curve is shown in Figure 4.

Figures 3 and 4 indicate that the single point or line located near the edge of the image may be ignored if their intensities are within the difference threshold according to the spatial concealment effect. Thus, these single point or line should be discarded during image enhancement.

3.3 Mach effect

Mach bands are an optical illusion consisting of an image of two wide bands, one light and one dark, separated by a narrow strip with a light-to-dark gradient. Human beings will perceive heteroptics, that is to say, they see two narrow bands of different brightness on either side of the gradient that are in fact not present in the original image.

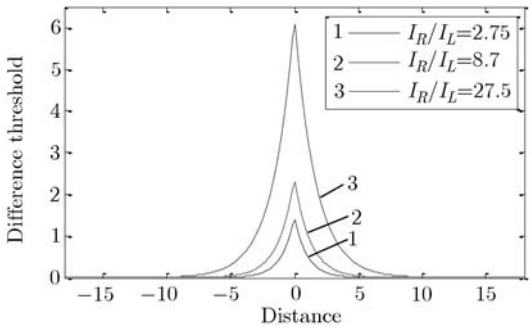

Figure 4 The curve of the difference threshold with the distance between the strip and the edge.

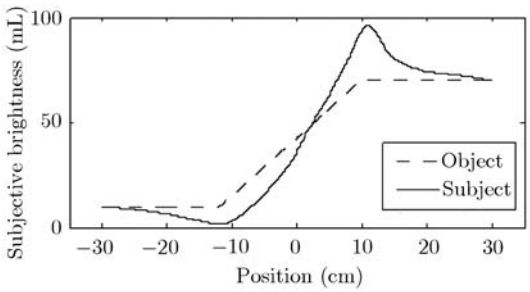

Figure 5 Schematic of Mach bands.

Table 1 Fitting models

Models	Expression	No. of parameters
Weibull	$Y = abx \wedge (b-1)\exp(-ax \wedge b)$	2
exp$N$	$Y = a_1\exp(b_1x) + \cdots + a_N\exp(b_Nx)$	$2N$
Fourier$N$	$Y = a_0 + a_1\cos(xp) + b_1\sin(xp) + \cdots + a_N\cos(Nxp) + b_N\sin(Nxp)$ where $p = 2\pi/[\max(x) - \min(x)]$	$2N$ +1
gauss$N$	$Y = a_1\exp\{-[(x-b_1)/c_1] \wedge 2\} + \cdots + a_N\exp\{-[(x-b_N)/c_N] \wedge 2\}$	$3N$
poly$N$	$Y = p_0x \wedge (N) + p_1x \wedge (N-1) + \cdots + p_N$	N+1
power$N$	$Y = a_1x \wedge b_1 + \cdots + a_Nx \wedge b_N + c$	$2N$+1
ratMN	$Y = \frac{p_1x \wedge M + \cdots + p_{M+1}}{x \wedge N + \cdots + q_N}$	$M + N$+1
sin$N$	$Y = a_1\sin(b_1x + c_1) + \cdots + a_N\sin(b_Nx + c_N)$	$3N$

Figure 5 plots a subject and object intensity of Mach effect. Comparison between Figure 3 and Figure 5 makes it clear that the difference threshold of spatial concealment appears as a pulse near the edge while that of Mach effect appears on either side of the gradient. This is the discrimination between spatial concealment effect and mach effect.

4 Modified Weber's law

Although Weber's law is the classical depiction of spatial concealment effect, a number of improvement schemes are proposed in the past years. Fullerton and Cattell indicated that the difference threshold should be inversely proportional with the square root of stimuli intensity. Guilford proposed a power law which assumes that the difference threshold is proportional with the n order power after calculating experiment data. The power law fits the data at the scotopic area whereas it does not match the data at the photopic area [7]. Steven [8] proposed the superior form which adds a bias into the model. Chen [9] suggested a piecewise function; however, it has a large error at the mesopic area.

In this paper a novel formula is proposed to depict the visual threshold effect. We do not explore the inherent rule by the visual physiological model but directly investigate the data fitting models [10] (see Table 1). In Table 1, x, Y are the predefined data, a, b, c, p, q are parameters of the model, M, N are relevant to the number of parameters.

The data are obtained from Konig and Grodhun [9]. The fitting rule is as follows: The error between the data and the fitting curve and the number of parameters should be as little as possible. The exp2 model is adopted since its has a high fitting data and only 4 parameters. The detailed model is

$$\Delta I/I = 0.003327 * I^{-1.011} + 0.06054 * I^{-0.2755}. \tag{6}$$

Then, a comparison of this model with classical models is shown in Figure 6. The x-axis is logarithmically scaled with the base number e.

From subjective vision, the Weber's law prevails only because of its simple form shown in Figure 6(a). Nevertheless, the gap between Weber's law and the experiment data is extremely large. Other methods

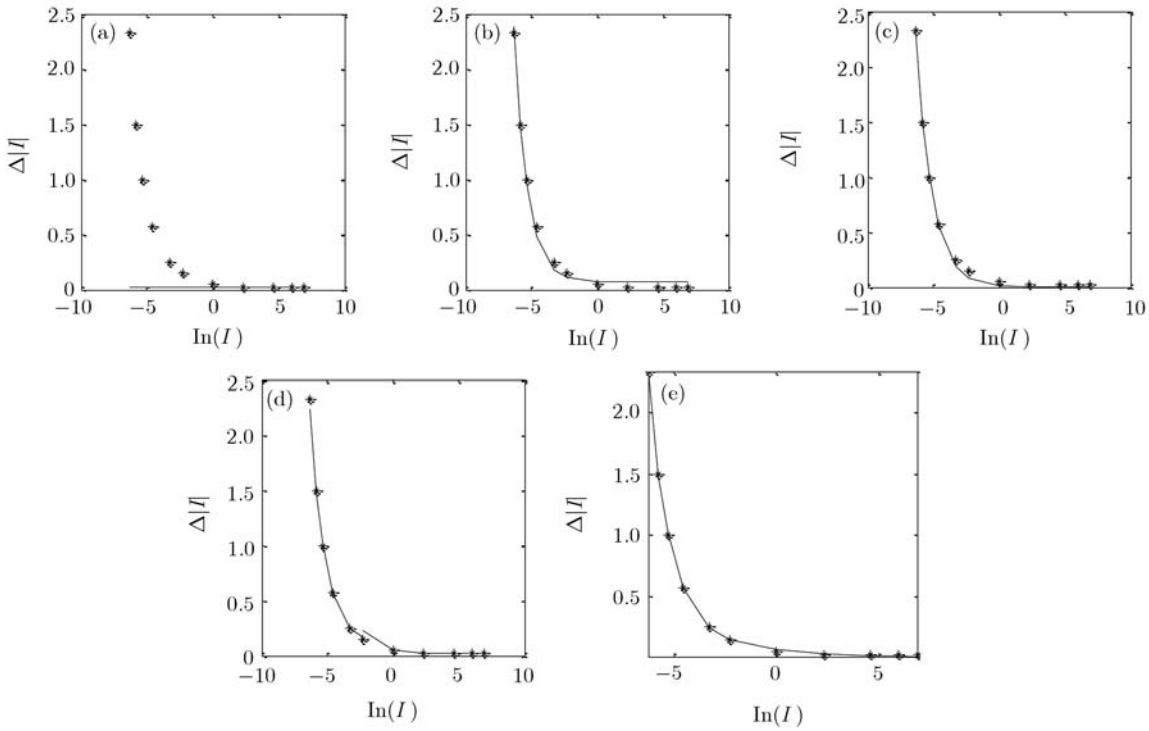

Figure 6 Comparison of different models of vision threshold effect. (a) Weber's law; (b) superior form; (c) Guiford's power law; (d) Chen's law; (e) our model.

Table 2 RMSE of models

Models	Expression	RMSE
Weber's law	$\Delta I/I = 0.0204$	0.8973
Superior form	$\Delta I(I + 0.0601) = 0.0695$	0.05711
Guilford's power law	$\Delta I/I^{0.1808} = 0.013$	0.0396
Chen's law	$(\Delta I/I)_{\text{Scotopic}} = 0.11 + 0.0077I^{-0.89}$ $(\Delta I/I)_{\text{Photopic}} = 0.02 + 0.033I^{-0.80}$	0.0370
Our model	$\Delta I/I = 0.003327I^{-1.011} + 0.06054I^{-0.2755}$	0.0097

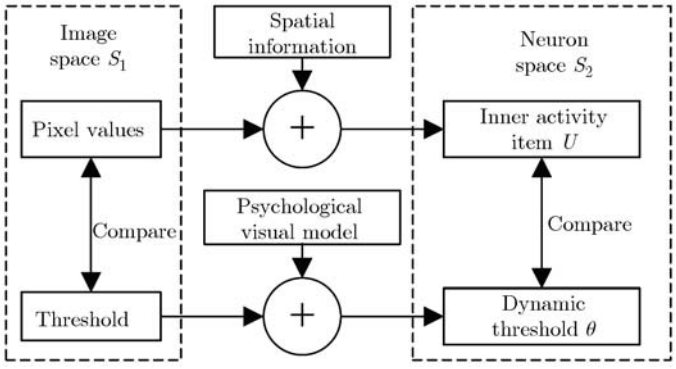

Figure 7 Mapping from image space to neuron space.

such as superior form, Guilford's power law, and Chen's law shown in Figure 6(b)–(d) also have an obvious shortcoming that the disparity cannot be narrowed, especially at the mesopic area. Figure 6(e) demonstrated that our fitting curve traverses all experiment data, and performs well even in the mesopic area.

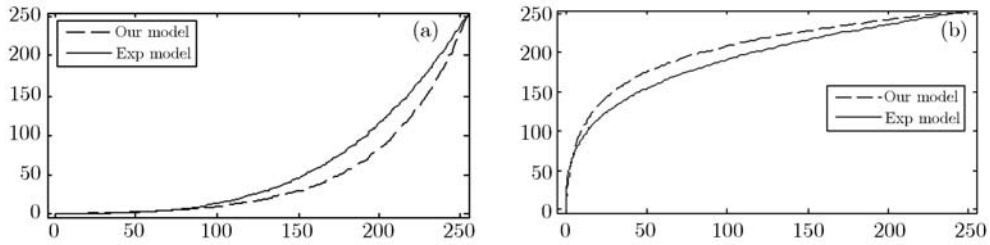

Figure 8 Comparison of difference intensity series between Weber's law and our model. (a) $I = T_1(n)$ & $I = T_2(n)$; (b) $n = T_1^{-1}(I)$ & $n = T_2^{-1}(I)$.

For objective judge, the RMSE calculated with each model are listed in Table 2, where the one with our model is the least. Although our model has just 2 parameters, the RMSE is only 1/3 of that with Chen's law.

5 Image global enhancement

The image space S_1 could be transformed into neuron space S_2 via PCNN, as shown in Figure 7 in detail.

Traditional enhancement is implemented in image space. The intensity of original image is compared with the predefined threshold, and the enhancement is done according to the results. No space information is explored except for the gray-level information.

Our method is executed in the neuron space. The information is mapped into the inner activity term U of the corresponding neurons. Meanwhile, the threshold θ is coupled with HVS model. Finally, comparison of U and θ will guide following enhancement.

5.1 Difference intensity series

In order to get the difference intensity series $I = T(n)$ where two adjacent intensities can be recognized by human eyes, the difference intensity series based on our VTE model described in (6) is obtained by replacing I by I_n and ΔI by $I_{n+1} - I_n$. The result is

$$I_{n+1} = I_n(1 + aI_n^b + cI_n^d), \tag{7}$$

where a=0.003327, $b = -1.011$, c=0.06054, and $d = -0.2755$. The iterations are done with the initial value of I_1 as 0.001 mL, and the curve of I versus n can be attained as $I = T_1(n)$ shown as the solid line in Figure 8(a).

The mapping function based on Weber's law is calculated as well for comparison, and the result is an exponential function

$$I_n = (1 + \alpha)^n I_0 \triangleq T_2(n) \tag{8}$$

with α=0.0204. Appropriate zoom parameters are chosen to make the two ends of $T_1(n)$ and $T_2(n)$ coincide. The mapping function is shown as the dashed line in Figure 8(a).

The inverse function of difference intensity series $n = T^{-1}(I)$ represents the HVS-based classification of gray-levels and is the foundation of image enhancement.

The inverse functions of $T_1(n)$ and $T_2(n)$ are drawn in Figure 8(b). The inverse function of eq. (7) is obtained as a numeric solution as $n = T_1^{-1}(I)$ while that of eq. (8) is deduced as $n = T_2^{-1}(I)$=$\log_{1+\alpha}(I_n/I_0)$ which is the well-known logarithmic enhancement model.

Traditional threshold of PCNN neurons decays in the way of $I = T_1(n)$, which may explains why PCNN can be applicable to images. In this paper, the threshold decays in a way similar to $I = T_2(n)$.

5.2 PCNN-based VTE

If the difference intensity series are directly used as the decay function of neurons of PCNN, the enhancement will be improved only a little since the space information is not employed. Thus, a simplified

PCNN model is proposed where the feedback input F is simplified into corresponding pixel values and the threshold is regulated to be infinite when the corresponding neuron is activated to guarantee the neuron not activate forever. The detailed formulas are

$$F_{ij}[n] = I_{ij}, \tag{9}$$

$$\theta_{ij}[n] = \begin{cases} \theta_1, & n = 0, Y[0] = 0, \\ g(n), & Y_{ij}[n-1] = 0, \theta_1 > \theta_0, \\ +\infty, & Y_{ij}[n-1] = 1. \end{cases} \tag{10}$$

Eq. (10) gradually reduces the dynamic threshold θ from θ_1 to θ_0. The neurons initialized as global restrain are gradually turned to global activation.

The process of PCNN is as follows:

Step 1: Estimate the gray-value range $[\theta_0, \theta_1]$ from the histogram. Construct a linear map S which projects the range $[\theta_0, \theta_1]$ to [1, 256].

Step 2: Simplify input F into the gray-value of the corresponding pixel. The element of the 3×3 inner link matrix W is assigned as the reciprocal of the square of the Euclidean distance.

Step 3: Determine the express of the decay of threshold:

$$g(n) = S^{-1}(T_1\{S[(\theta_0 - \theta_1)n/NP + \theta_1]\}). \tag{11}$$

Here NP denotes the times of iteration, which usually chooses 500–2000. The term $(\theta_0 - \theta_1)n/NP + \theta_1$ denotes the linear decay rule in the neuron space. Operator S projects its value range into image space, namely [1, 256]. Operator T_1 modifies the decay rate from linear scale to nonlinear scale as shown in Figure 8(a). Operator S^{-1} projects the range back to the neuron space.

Step 4: Run the PCNN, and record the output image Y at time i as $Y[i]$.

Step 5: Accumulate $Y[i]$ as

$$S[j] = \sum_{i=1}^{j} Y[i], \tag{12}$$

where $S[j]$ is black-white image since the support areas (positions where value equals 1) in $Y[i]$s with different i are not overlapped. The support area of $S[j]$ gradually proliferates as time passes.

Step 6: Compute the sum of $S[j]$. The result is an image within the gray-level [1, NP]. Project it linearly into the image space,

$$Enh = Sum(S[j])/NP * 256. \tag{13}$$

And the Enh is the enhanced image.

6 Image local enhancement

Section 5 has discussed the global enhancement. This section will continue to investigate the local enhancement via PCNN.

6.1 Application of SCE

Spatial concealment effect can mainly be used for double-edges whose gray-values do not far differ from their background, and then, those double-edges could be median-filtered. The schematic diagram is shown in Figure 9.

Firstly, we detect the double edges in original image. In the second stage, we check whether the difference in the absolute value of the intensity between the edges and their background is higher than the threshold. If higher, human eyes can perceive the edges and they should be kept unchanged; otherwise, they can be median-filtered since human eyes cannot perceive their existence.

The advantages of the preprocessing are as follows:

• It does not affect human visions.

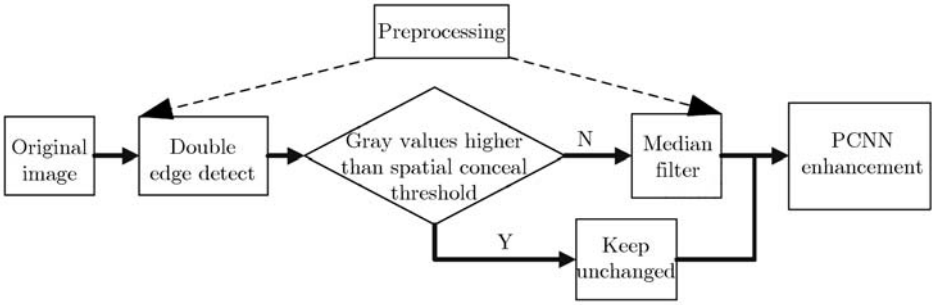

Figure 9 Preprocessing based on SCE.

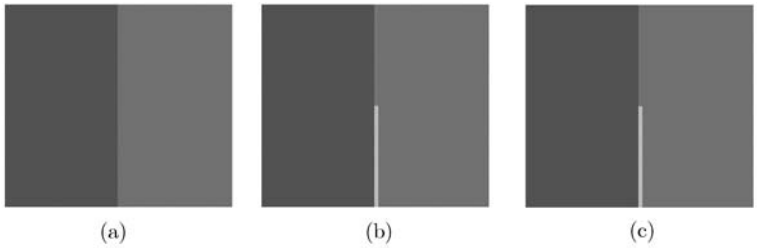

Figure 10 Test images validating SCE (JPEG). (a) Single-edge (1292B); (b) append a vertical line (1330B); (c) preprocessed image (1326B).

- The storage for the preprocessed image is less.
- The noise and false-edge can be smoothed.
- Those noise and false-edges may influence posterior processings.
- In all, the preprocessing can be regarded as computer vision oriented enhancement.

We take two examples to validate our method. Figure 10(a) is an image consisting of two wide bands, namely a single-edge. The gray-values of the left area and right area are 160 and 180 respectively. Figure 10(b) adds a vertical line which comprises an upper part whose intensity is 185 and a lower part whose intensity is 220.

The upper part of the vertical line is higher than its background; however, it does not exceed the threshold. Meanwhile, the lower part is high enough to exceed both the background and the threshold. Thus, only the lower part can be perceived by human eyes, and both upper and lower part can be perceived by computer visions.

Figure 10(c) is a preprocessed image. The upper part of the vertical line in the middle has been filtered with gray-value 180.

In Figure 10(b) and (c), the storage room of preprocessed image is 1326B, 4B less than that of original image. At the same time, human eyes cannot distinguish the two images.

The second example is Lena, which is supposed to be slightly stained and hardly perceivable by human eyes. The enhancement may be unnecessary for human vision but indispensable for computer vision.

Figure 11(a)–(c) show Lena, stained Lena, preprocessed Lena and their corresponding edges. If the false-edges caused by noises, seen in Figure 11(b), are not filtered, they will cause a rapid increase in storages. Moreover, computers may consider these false-edges as normal ones, which will severely obstruct the later processing.

The two examples make it explicit that the enhancement based on SCE oriented for computer vision is consequent.

6.2 Application of Mach effect

Mach effect is embedded into the neurons of PCNN. The concept is as follows: Suppose that there are two adjacent pixels with similar gray-values and high chance of synchronous activations, and the pixels in enhanced images are close to each other. Otherwise, the synchronous activation is strained leading to large difference in gray-values of enhanced image.

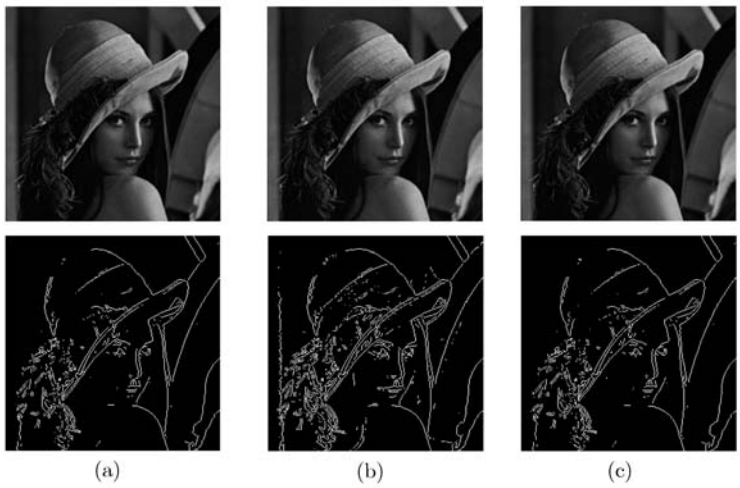

Figure 11 Lena image validating SCE (LZW). (a) Lena (89088B) and its edges; (b) stained Lena (220796B) and its edges; (c) preprocessed image (102756B) and its edges.

Considering that the source of Mach effect is the lateral inhibition of visual nerve system, PCNN is coupled with lateral inhibition to mimic real visual nerve system. The detailed process goes in two steps [11]:

Step 1: Add a lateral inhibition signal R_{ij} as a bias of threshold at every neuron

$$\theta_{ij}[n] = \theta'_{ij}[n] + R_{ij}, \tag{14}$$

where

$$R_{ij} = f(1/\beta_{ij}), \tag{15}$$

$\theta'_{ij}[n]$ stands for the new threshold to indicate that the effect of R_{ij} is to control and regulate the value of the threshold.

Step 2: Replace link parameter β is with space-variant. The definition of β_{ij} is

$$\beta_{ij} = 1/9 \sum_{m=i-1}^{i+1} \sum_{n=j-1}^{j+1} \gamma_{mn}. \tag{16}$$

Here

$$\gamma_{mn} = \begin{cases} 1/(I_{mn} - I_{ij})^2, & I_{mn} \neq I_{ij}, \\ 100, & I_{mn} = I_{ij}. \end{cases} \tag{17}$$

γ_{mn} denotes the contrast of the pixel gray-value in ith row, jth denotes the column to its ambient pixels, and β_{ij} is the average of these 9 gray-values.

If the pixels in ith row and jth columns are located at edges, difference between them and surrounding pixels→ the less β_{ij} → the less U_{ij} (see eq. (3))→the larger R_{ij} (see eq. (15))→ the larger θ_{ij} (see eq. (14))→ neurons are not easily to be activated synchronously→ neurons on either side of the edge activate asynchronously→ the larger the difference of the gray-values of the corresponding pixels in enhanced image.

Among common color space models, HIS is fit for HVS since the I component is independent of the image color information, and the H and S components are closely correlated with the style of perceiving color information via human eyes.

The methods for converting RGB model into HIS model involve cylinder transform, hexagonal pyramid transform, sphere transform, and triangular transform. On the one hand, the geometric features of the fused image via triangular transform and cylinder transform are better; on the other hand, the triangular transform takes the best information and standard variance. Thus, triangular transform is adopted; its

forward and inverse transform are as follows:

$$\begin{cases} I = \dfrac{R+G+B}{3},\ H = \dfrac{G-B}{3(I-B)},\ S = 1-\dfrac{B}{I},\ R > B \leqslant G, \\ I = \dfrac{R+G+B}{3},\ H = \dfrac{B-R}{3(I-R)+1},\ S = 1-\dfrac{R}{I}, \\ I = \dfrac{R+G+B}{3},\ H = \dfrac{R-G}{3(R-G)+2},\ S = 1-\dfrac{G}{I},\ B > G \leqslant R. \end{cases} \tag{18}$$

$$\begin{cases} R = I(1+2S-3SH),\ G = I(1-S+3SH),\ B = I(1-S),\ 0 \leqslant H < 1; \\ R = I(1-S),\ G = I(1+5S-3SH),\ B = I(1-4S+3SH); \\ R = I(1-7S+3SH),\ G = I(1-S),\ B = I(1+8S-3SH), 2 \leqslant H < 3. \end{cases} \tag{19}$$

6.3 Component enhancement

The enhancement of I component can directly follow the above method since it stands for gray-values.

To enhance the color information, the S component should be exponentially stretched [12],

$$\tilde{S} = S^{\lambda}. \tag{20}$$

Here λ is the stretch factor used for determining the level of saturation.

6.4 Implementation

Step 1: Transform images of RGB space into HIS space with eq. (18).
Step 2: Enhance the I component using PCNN.
Step 3: Stretch the S component with eq. (20).
Step 4: Normalize I and S components.
Step 5: Transform the HSV space back to the RGB space again via eq. (19).

7 Experiments of gray-level image enhancement

7.1 Comparison with log enhancement

The standard test image "Cameraman" is adopted, and the parameters of PCNN are chosen as α_L= 0.06931, α_θ=0.0055, β=0.05, V_L=1.00, θ_0=1, θ_1=256, and NP=1024.

Log enhancement can only make the image brighter, but does no help to enhance the contrast of its details.

However, our method can accomplish the task. The pocket and the clasp of the sleeves can be seen clearly. The most enhanced details are the sky and lawn, where the internal gray-level undulation looks like waves.

Sobel edge-detector is employed to detect the three images in Figure 12(a)–(c) with the detect threshold 0.15. The edges detected, as shown in Figure 12(c), contain more information such as the contour of distant building and the texture of near lawn.

7.2 Comparison with HE enhancement

Figure 13 shows that the HE enhancement stretches the contrast of the original image, but brings the "gray-level loss" in processed image.

Our method do not produce any "gray-level loss" since the enhanced picture in image space is mapped from the neuron space where the range of gray-level is as high as 1024.

In Figure 14 we use Tire image to compare our method and HE again, which demonstrates that the histogram of our enhancement is more equalized and contains enough gray-levels.

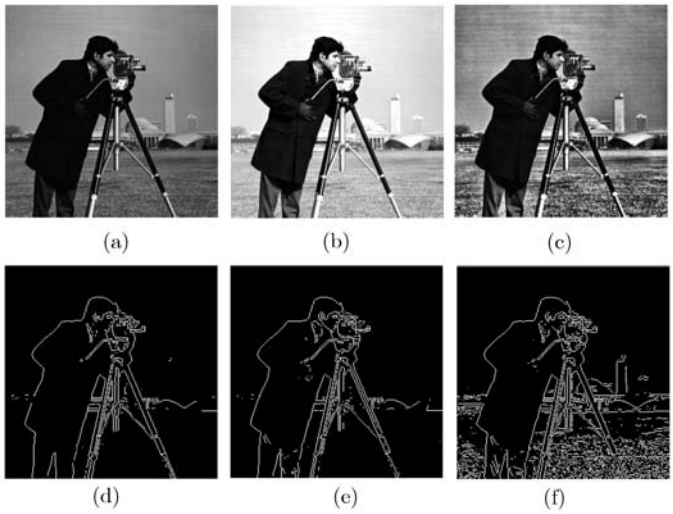

Figure 12 Comparison with log enhancement. (a) Original image; (b) log enhancement; (c) our enhancement; (d) edge of original image; (e) edge of log enhancement; (f) edge of our enhancement.

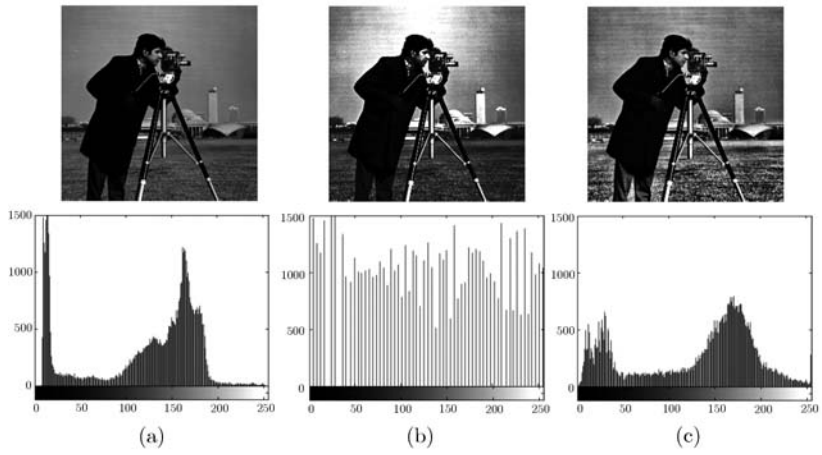

Figure 13 Comparison with HE enhancement of Cameraman image. (a) Original image and its histogram; (b) HE enhancement and its histogram; (c) our enhancement and its histogram.

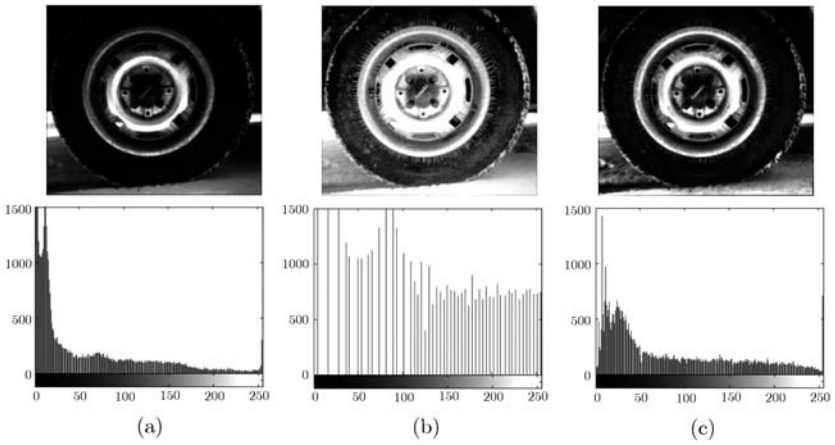

Figure 14 Comparison of HE enhancement of Tyre images. (a) Original image and its histogram; (b) HE enhancement and its histogram; (c) our enhancement and its histogram.

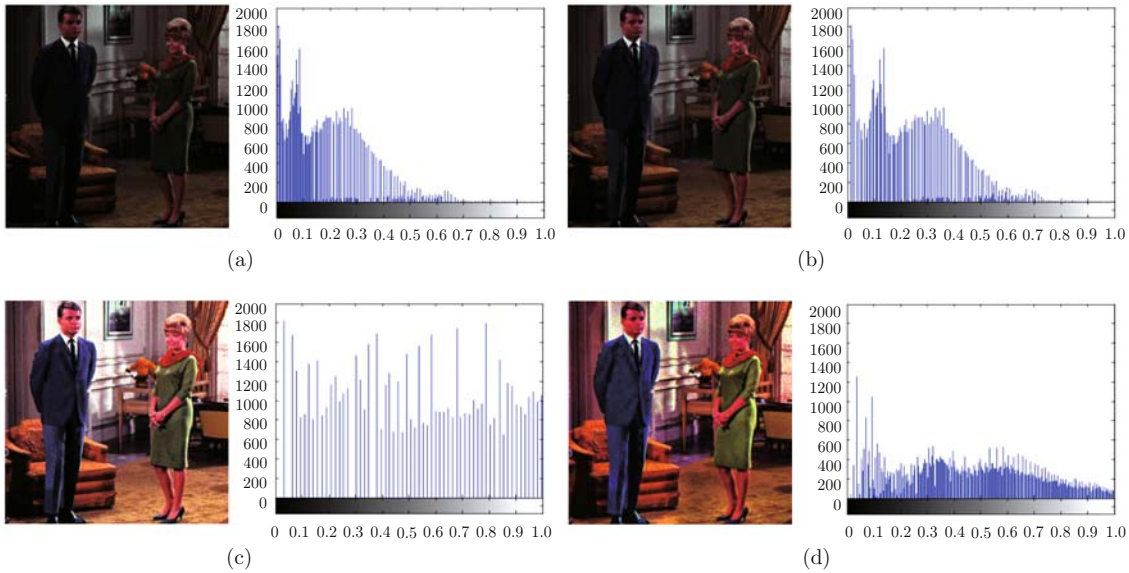

Figure 15 Couple image enhancement. (a) Original image and its histogram; (b) log enhancement and its histogram; (c) HE enhancement and its histogram; (d) our enhancement and its histogram.

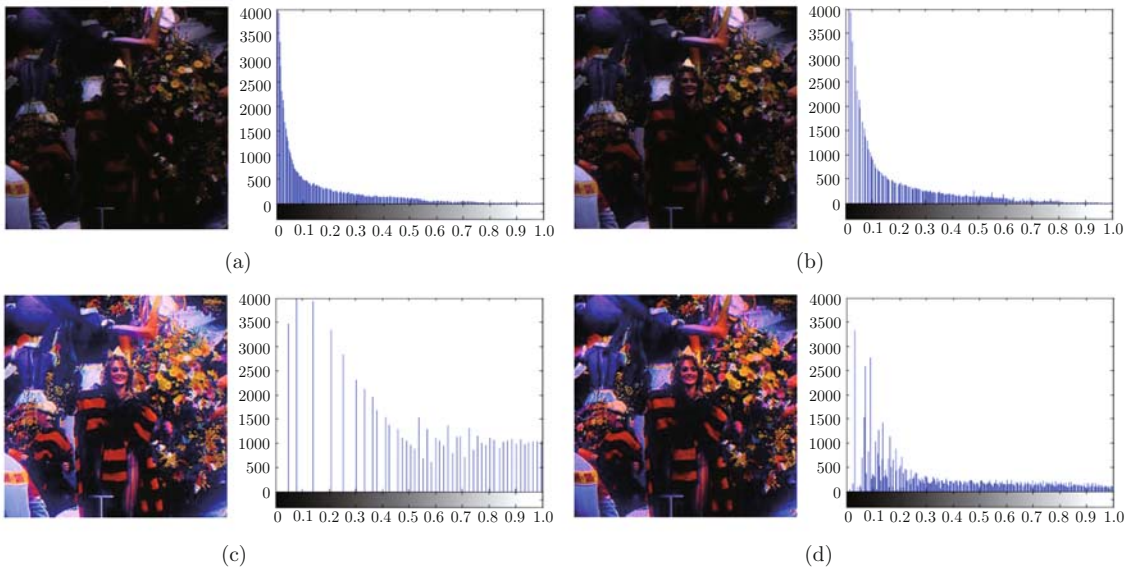

Figure 16 Carnev image enhancement. (a) Original image and its histogram; (b) log enhancement and its histogram; (c) HE enhancement and its histogram; (d) our Enhancement and its histogram.

Table 3 Comparison of serial computations

Image	Enhancement algorithm		
	Log	HE	Our method
Cameraman	0.033	0.0056	5.76
Tyre	0.031	0.0053	6.19
Couple	0.034	0.0068	6.12
Carnev	0.036	0.0064	5.95

8 Color image enhancement

Figures 15 and 16 give comparison on enhancement of "Couple" and "Carnev" images with λ set at 0.5.

The object and background in our enhanced images are more distinct, more brilliant, and more evident at contours especially. Observing the faces in both images, we can discover that the one in log enhance-

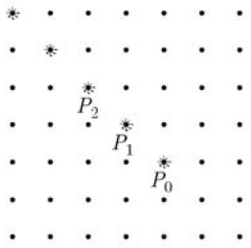

Figure 17 The multi-processor strategy. P, the processor; •, the pixel; *, the position of processor.

Table 4 Computation time of two parallel means

Image	Multi-processor	Circuitization
Cameraman	5.64e-2	8.42e-5
Tyre	5.79e-2	8.34e-5
Couple	6.12e-2	8.68e-5
Carnev	6.11e-2	8.71e-5

ment is obscure, the one in HE enhancement seems freezing and over-smooth, and the one in our enhancement appears exquisite with polished color.

9 Time analysis

9.1 Serial computation

The time-consuming are tested using the Matlab on IBM P4 of 1.86 GHz/504 MB.

As seen in Table 3, the computation time of our method is about 5–6 s with a 256×256 image, much longer than those of log enhancement and HE, and depends on unnecessary training of PCNN. However, it seems acceptable and worthy.

9.2 Parallel computation

Another reason for choosing PCNN rests with the intrinsic parallelism. Two types of parallel computation are described as follows.

The first means is to use multi-processor. By eqs. (1)–(5), all information of a pixel, namely $L[n]$, $F[n]$, $U[n]$, $\theta[n]$, and $Y[n]$, can be calculated by $Y[n-1]$ of its peripheral 3×3 neurons.

Thus, a strategy of multi-processor is depicted in Figure 17. Use the processors to scan the image row by row. If the 0th processor finishes the scan of a row and one pixel, the 1st processor commences its journey, and so on. If there are 256 processors for a 256×256 image enhancement, the computation time will be only 1/255 of that in serial computation.

The second means is to put PCNN in electronic circuit such that the neurons in PCNN can work synchronously. The computation will only be related to the iterative times.

We use virtual reality toolbox to simulate these two methods, and the results are shown in Table 4.

Our method is superior to the traditional methods since the neural network is natural for parallelism.

10 Conclusions

A novel image enhancement approach based on HVS and PCNN is presented in this paper. The main innovations are as follows:

(1) We propose a novel fitting model to describe the visual threshold effect, which excels classical Weber's law.

(2) We change the threshold of the neuron in PCNN into $T_1(n)$, which makes the enhanced image more smooth.

(3) We use preprocessing to simulate the spatial conceal effect, thus wiping off the unaware double-edge and saving the storages.

(4) We introduce lateral inhibition into PCNN to simulate the Mach effect, thus improving the contrast.

(5) We simplify the model of PCNN and reduce the iterative times to only 500–2000 steps.

(6) The model can be generalized to color image.

The future researches include the following aspects:

(1) Although the corrected Weber's law fits the data better, the formula lacks realistic physiological sense.

(2) A circuital material goods [13] should be created to validate our method.

(3) We will embed our method into other techniques, such as image fusion [14], image segmentation [15], image restoration [16], etc.

Acknowledgements

This work was supported by the National Natural Science Foundation of China (Grant No. 60872075), the National Technical Innovation Project Essential Project Cultivate Project (Grant No. 706928), and the Natural Science Fund of Jiangsu Province (Grant No. BK2007103).

References

1 Kim J K, Kim L S. An advanced contrast enhancement using partially overlapped subblock histogram equalization. IEEE Trans Circ Vid Tech, 2001, 11: 475–484

2 Chang D C, Wu W R. Image contrast enhancement based on a histogram transformation of local standard deviation. IEEE Trans Med Imag, 1998, 17: 518–531

3 Li T L, Sundarehan M K. Adaptive image contrast enhancement based on human visual properties. IEEE Trans Med Imag, 1994, 13: 573–586

4 Eckhorn R, Reitboeck H H, Arndt M, et al. Feature linking via synchronization among distributed assemblies: simulation of results from cat cortex. Neur Comput, 1990, 2: 293–307

5 Zhang Y D, Wu L N. Image segmentation based on 2D Tsallis entropy with improved pulse coupled neural networks (in Chinese). Southeast Univ J (Nat Sci Ed). 2008, 38: 579–584

6 Zhang Y D, Wu L N. Improved image filter based on SPCNN. Sci China Ser F-Inf Sci, 2008, 51: 2115–2125

7 Augustin T. The problem of meaningfulness: Weber's law, Guilford's power law, and the near-miss-to-Weber's law. Math Social Sci, 2009, 57: 117–130

8 Stevens S S. On the psychophysical law. Psych Rev, 1957, (64): 173

9 Chen W X. An analytical expression of weber ratio (in Chinese). Acta Pshych Sin. 1996, 28: 419–424

10 Zhang Y D, Wu L N, Wei G. A novel fitting formula for spatial conceal effect (in Chinese). Chin Opt Appl Opt, 2008, 1: 70–74

11 Ma Y D, Li L, Zhan K, et al. PCNN and Digital Image Processing (in Chinese). Beijing: Science Press. 2008

12 Huang K Q, Wang Q, Wu Z Y, et al. Multi-scale color image enhancement algorithm based on human visual system (in Chinese). J Image Graph, 2003, 8: 1242–1246

13 Qiao F, Yang H Z, Huang G, et al. Implementation of low-swing different interface circuits for high-speed on-chip asynchronous interconnection. Sci China Ser F- Inf Sci, 2008, 51: 975–984

14 Liu B, Peng J X. Multi-spectral image fusion method based on two channels non-separable wavelets. Sci China Ser F-Inf Sci, 2008, 51: 2022–2032

15 Liu F. Diffusion filtering in image processing based on wavelet transform. Sci China Ser F-Inf Sci, 2006, 49: 494–503

16 Zhang Y D, Wu L N. Improved immune algorithm for image restoration (in Chinese). Opt Precis Eng, 2009, 17: 417–425